Multiband and Wideband Self-Multipath Decoupled Antenna Pairs

Aofang Zhang, *Member, IEEE*, Kunpeng Wei, *Senior Member, IEEE*, and Zhijun Zhang, *Fellow, IEEE*

***Abstract*— We propose a series of closely spaced self-multipath decoupled antenna pairs that are capable of realizing self-decoupling performance from a single band to four bands for 5G mobile terminals. First, we propose a self-multipath counteraction method by building multiple coupling paths on the radiating branch of one of the antennas, where the coupling energy passing through the multiple coupling paths could be counteracted at the feeding ports. Based on this principle, two types of single-band self-multipath decoupled antenna pairs are constructed with the shorted end and the open end without using any additional decoupling structures. Then, a dual-band and wideband self-multipath decoupled antenna pair is designed by combining the multipath of such two types of single-band self-multipath decoupled antenna pairs. Finally, a four-band and wideband self-multipath decoupled antenna pair is constructed to further widen the decoupling bandwidth based on the dual-band self-multipath decoupled antenna pair. Both simulated and measured results show that the four-band antenna pair can be self-decoupled at four bands with the isolation more than 20 dB over entire N77, N78, and N79 bands, demonstrating excellent multiband and wideband self-decoupling performance. The proposed self-multipath counteraction method, with the merits of simple antenna structure and wideband self-decoupling performance, should provide significant application values for the very compact and wideband multiple-input multiple-output (MIMO) systems.**

***Index Terms*— Antenna decoupling, multiband and wideband, self-decoupled, self-multipath counteraction.**

I. Introduction

THE multiple-input multiple-output (MIMO) technique has been commercialized in 5G mobile terminals in recent years, since it has been proven to be able to multiply the throughput rate of the transmitting data [1]. However, as more and more antennas are required in a 5G mobile terminal, multiple antennas have to be placed closely in the limited available space, which may degrade the isolation or correlation performance, thus leading to the deterioration of the throughput rate. Especially, in order to minimize the number of antennas, multiband and wideband antennas are designed to support more 5G new radio (NR) bands, such as integrating entire N77 (3.3–4.2 GHz), N78 (3.3–3.8 GHz), and N79 (4.4–5.0 GHz) bands into a single antenna, which would further increase the difficulty in the design of compactly spaced antennas. Therefore, it would be of great significance to design multiband and wideband MIMO antennas with the extremely compact distance while having better isolation performance for 5G and future 6G mobile terminals.

To solve the coupling problems, plentiful decoupling techniques have been proposed by adding extra decoupling structures or components in previous studies [2], [3], [4], [5], [6], [7], [8], [9], [10], [11], [12], [13], [14], [15], [16], [17], [18], [19], such as defected ground structures [2], [3], [4], decoupling networks [5], [6], [7], [8], parasitic scatterers [9], [10], neutralization lines [11], [12], [13], and lumped elements [14], [15], [16], [17], [18], [19]. Among these studies, some multiband decoupling structures have been demonstrated to improve the decoupling bandwidth [10], [13], [18], [19]. In [10], four parasitic scatterers are added between two antennas to block the coupling energies at four-frequency bands. In [13], three neutralization lines are connected between two antennas to reduce the mutual coupling at three-frequency bands. In [18] and [19], by inserting lumped elements or connecting lines, closely spaced open-slot antenna pairs with face-to-face or back-to-back configuration could be decoupled at two-frequency bands. These studies have demonstrated excellent decoupling performance for the design of multiband antenna pairs. However, extra decoupling structures or components may occupy the limited available space, and it is difficult to obtain a high isolation, e.g., 20 dB, for closely spaced antenna pairs over a wideband range.

To further squeeze the available space for MIMO antennas, self-decoupled antenna pairs have been shown to be capable of effectively achieving better isolation with a compact distance without adding extra decoupling structures [20], [21], [22], [23], [24], [25], [26], [27], [28], [29], [30], [31], [32]. For example, by placing symmetrical antenna pairs together using orthogonal modes, such as common mode (CM) and differential mode (DM), the inherent characteristics of the orthogonal modes could easily generate the high isolation of the antenna pairs [20], [21], [22], [23], [24], [25]. However, by tuning CM and DM impedances to be similar states based on the mode cancellation method, both CM and DM can be excited and canceled out, leading to the self-decoupling performance of

Manuscript received 4 January 2023; revised 15 March 2023; accepted 9 April 2023. Date of publication 19 April 2023; date of current version 7 July 2023. This work was supported by the Beijing Science and Technology Plan Project under Contract Z211100004421011. *(Corresponding author: Kunpeng Wei.)*

Aofang Zhang is with Honor Device Company Ltd., Xi'an 710000, China (e-mail: aofangzhang@foxmail.com).

Kunpeng Wei was with Honor Device Company Ltd., Beijing 100095, China. He is now with Xiaomi Communications Company Ltd., Beijing 100085, China (e-mail: weikunpeng_2013@tsinghua.org.cn).

Zhijun Zhang is with the Beijing National Research Center for Information Science and Technology (BNRist), Tsinghua University, Beijing 100084, China.

Color versions of one or more figures in this article are available at https://doi.org/10.1109/TAP.2023.3267177.

Digital Object Identifier 10.1109/TAP.2023.3267177

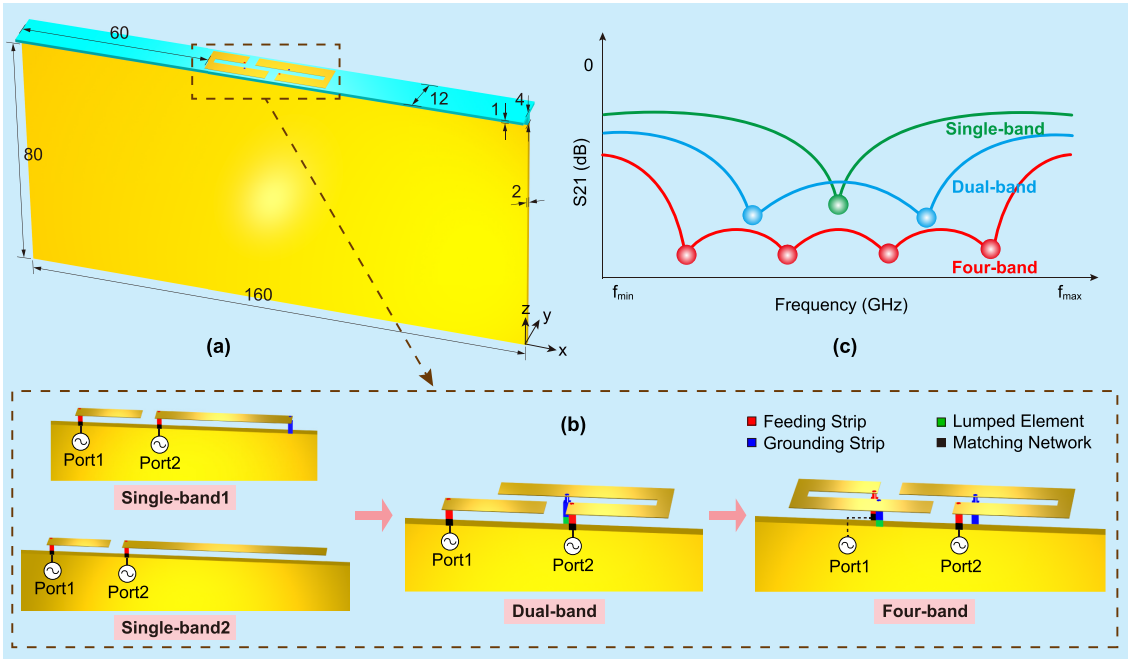

Fig. 1. Configuration of the proposed self-multipath decoupled antenna pair. (a) Structure of the self-multipath decoupled antenna pair. (b) Evolution of the self-multipath decoupled antenna pair from the single-band to the four-band self-decoupling performance. (c) Demonstration of the coupling coefficients from single-band to four-band self-decoupling performance.

the symmetrical antenna pairs [26], [27], [28]. Among these studies, some dual-band self-decoupled antenna pairs also have been demonstrated [23], [30]. In [23], lumped filters are inserted in a compactly spaced antenna pair with orthogonal modes to have different effective electrical sizes for high-band and low-band, respectively, leading to the dual-band operation and decoupling performance. In [30], by setting high-band and low-band radiating branches separately, dual-band self-decoupled antenna pair can be obtained with the shared feeding and grounding branches. However, symmetrical structures are strictly required of these self-decoupled antenna pairs to have a better decoupling performance, and it may be difficult to further obtain multiband self-decoupling performance for more than two bands.

In this article, we propose a self-multipath counteraction method that is different from previous studies for self-decoupled antennas. Based on this method, we design a series of self-multipath decoupled antenna pairs from a single band to four bands, thus realizing wideband self-decoupling performance. Especially, we show that the four-band antenna pair with very close distance can be self-decoupled at four bands with the isolation more than 20 dB in the −6 dB impedance bandwidth from 3.1 to 5.1 GHz, covering entire N77, N78, and N79 bands. Compared with the previous studies, the proposed design has the advantages and features of that: 1) it is self-decoupled without using any additional decoupling structures; 2) it does not require symmetrical antenna structures; 3) multiband (more than dual bands) and wideband decoupling performance can be realized; and 4) excellent decoupling performance more than 20 dB of isolation can be obtained for closely spaced antennas.

This article is organized as follows. In Section II, the self-multipath counteraction method is proposed. In Section III, two types of single-band self-multipath decoupled antenna pairs are designed. In Section IV, the dual-band self-multipath decoupled antenna pair is presented. In Sections V and VI, the four-band self-multipath decoupled antenna pair is demonstrated and the experiment is carried out, respectively. Finally, conclusion is drawn in Section VII.

II. Design Principle

Fig. 1(a) shows the structure of our proposed self-multipath decoupled antenna pair. The antenna pair is attached to an FR4 dielectric board ($\varepsilon_r = 4.4$ and loss tangent $= 0.02$) and mounted on a metallic ground plane to mimic a mobile terminal. Fig. 1(b) demonstrates the evolution of our proposed self-multipath decoupled antenna pair, where the dual antennas in all cases are placed with extremely close distance without using any additional decoupling structures. Through such a design procedure, as shown in Fig. 1(c), the self-decoupling performance from the single-band to the four-band can be easily achieved, thus realizing a very wideband self-decoupling performance of our proposed self-multipath decoupled antenna pair.

To interpret the working mechanism of the multiband self-decoupling performance, we start with the design of the single-band self-multipath decoupled antenna pairs through our proposed self-multipath counteraction method.

As shown in Fig. 2(a) and (b), we propose two types of single-band self-multipath decoupled antenna pairs with the shorted end and the open end. For the first single-band self-multipath decoupled antenna pair with the shorted end in Fig. 2(a), the feeding port of Ant2 is placed close to Ant1, and the right end of Ant2 is shorted. When Ant1 is excited, there are mainly two self-decoupling paths on Ant2 being created to couple the energy from Ant1 to Port2. Path1 is the direct

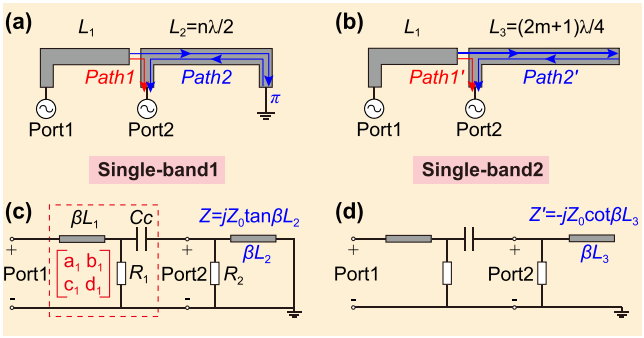

Fig. 2. Self-decoupling principle of two types of single-band self-multipath decoupled antenna pairs. (a) and (b) Schematic diagrams of the self-decoupling paths for single-band1 and single-band2 self-multipath decoupled antenna pairs. (c) and (d) Equivalent circuits of the single-band1 and single-band2 self-multipath decoupled antenna pairs.

coupling path from the end of Ant1 to Port2. Path2 is the transmission path from the end of Ant1 to the shorted end of Ant2 with the superposition of the reflection path back to Port2, where a reflection phase of π would be introduced at the shorted end of Ant2. Therefore, the coupling powers from such two self-decoupling paths have the phase difference of

$$\text{Phase(path2)} - \text{Phase(path1)} = 2 * \beta L_2 + \pi \tag{1}$$

where L_2 is the length of Ant2, $\beta = 2\pi/\lambda$ is the phase constant, and λ is the wavelength in the substrate. When

$$L_2 = n\lambda/2, \quad n = 1, 2, 3 \tag{2}$$

we have

$$\text{Phase(path2)} - \text{Phase(path1)} = (2n+1)\pi. \tag{3}$$

Therefore, when (2) is satisfied, the coupling powers from path1 and path2 could be counteracted at Port2, and the self-multipath decoupled antenna pair in Fig. 2(a) could be self-decoupled.

However, the amplitudes of the two paths may be different due to that a part of the power of path2 would be radiated out through Ant2, which would result in the variation of the decoupling level but not decoupling frequency.

It should be noted that the other areas where the two paths pass through, such as the ground and Ant1, are not drawn in Fig. 2(a). And this is because they are in the common area of both path1 and path2, leading to that the phase difference in (3) would not be affected.

Similarly, as shown in Fig. 2(b), when the end of Ant3 is open for the second single-band self-multipath decoupled antenna pair, the reflection phase would be zero at the open end, and we have

$$\text{Phase(path2}') - \text{Phase(path1}') = 2 * \beta L_3. \tag{4}$$

When

$$L_3 = (2m+1)\lambda/4, \quad m = 0, 1, 2 \tag{5}$$

we have

$$\text{Phase(path2}') - \text{Phase(path1}') = (2m+1)\pi. \tag{6}$$

In such a situation, we can also obtain the self-decoupling performance of the second single-band self-multipath decoupled antenna pair in Fig. 2(b).

In order to further illustrate the self-decoupling mechanism of the self-multipath counteraction method, Fig. 2(c) and (d) demonstrates the equivalent circuits of the self-multipath decoupled antenna pairs.

In Fig. 2(c), R_1 and R_2 represent the radiation loss of Ant1 and Ant2, respectively, C_c represents the coupling effect between Ant1 and Ant2, and the transmission lines of βL_1 and βL_2 represent the antenna radiating branches of Ant1 and Ant2, respectively. For a shorted transmission line of βL_2, the input impedance is $Z = jZ_0 \tan(\beta L_2)$, where Z_0 is the characteristic impedance of the transmission line. The transmission matrix from Port1 to Port2 can be expressed as [33]

$$\begin{bmatrix} A & B \\ C & D \end{bmatrix} = \begin{bmatrix} a_1 & b_1 \\ c_1 & d_1 \end{bmatrix} \begin{bmatrix} 1 & 0 \\ \frac{1}{R_2} & 1 \end{bmatrix} \begin{bmatrix} 1 & 0 \\ \frac{1}{jZ_0\tan(\beta L_2)} & 1 \end{bmatrix} \tag{7}$$

where $[a_1 \ b_1 \ c_1 \ d_1]$ refers to the total transmission matrix consisting of βL_1, R_1, and C_c. From (7), we have

$$\begin{cases} A = a_1 + b_1/R_2 - jb_1\cot(\beta L_2)/Z_0 \\ B = b_1 \\ C = c_1 + d_1/R_2 - jd_1\cot(\beta L_2)/Z_0 \\ D = d_1. \end{cases} \tag{8}$$

The coupling coefficient of S_{21} can be expressed as

$$S_{21} = \frac{2}{A + B/Z_0 + CZ_0 + D}. \tag{9}$$

Therefore, we can obtain

$$|S_{21}| = \frac{2}{\sqrt{E^2 + F^2\cot^2(\beta L_2)}} \tag{10}$$

where

$$\begin{cases} E = a_1 + b_1/R_2 + b_1/Z_0 + c_1Z_0 + d_1Z_0/R_2 + d_1 \\ F = b_1/Z_0 + d_1. \end{cases} \tag{11}$$

When

$$L_2 = n\lambda/2, \quad n = 1, 2, 3 \tag{12}$$

we have $|S_{21}| = 0$ and the self-decoupling performance can be obtained in Fig. 2(c).

For an open ended transmission line of βL_3 in Fig. 2(d), the input impedance is $Z' = -jZ_0\cot(\beta L_3)$. Similarly, we can obtain

$$|S'_{21}| = \frac{2}{\sqrt{E^2 + F^2\tan^2(\beta L_3)}}. \tag{13}$$

When

$$L_3 = (2m+1)\lambda/4, \quad m = 0, 1, 2 \tag{14}$$

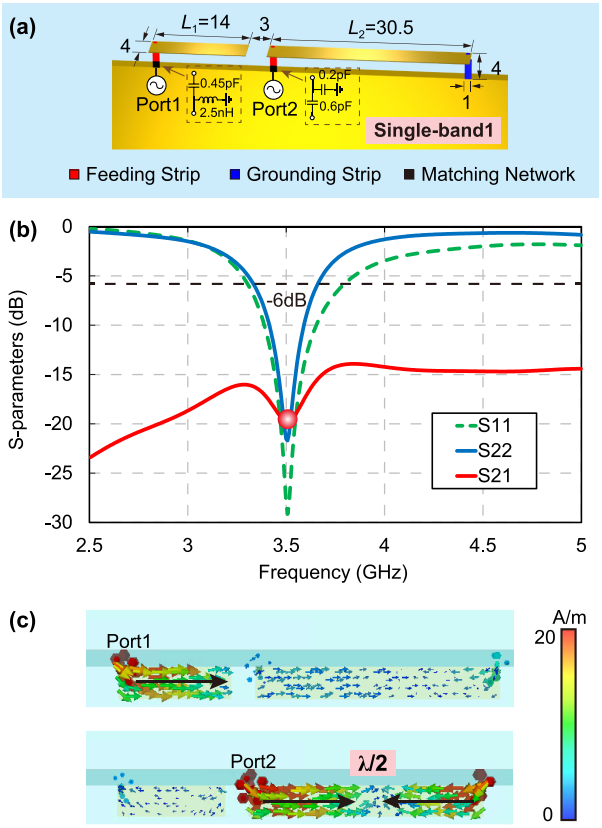

Fig. 3. Single-band1 self-multipath decoupled antenna pair. (a) Antenna structure. (b) S-parameters. (c) Surface current distributions at 3.5 GHz.

we have $|S'_{21}| = 0$ and the self-decoupling performance can be obtained in Fig. 2(d).

From (12) and (14) in the equivalent circuits, we can obtain the same self-decoupling conditions as (2) and (5).

However, we can also observe from (7) that the self-multipath counteraction effect of the proposed antenna pairs would not be affected by a_1, b_1, c_1, and d_1. Therefore, Ant1 can be changed to other type antennas.

III. Single-Band Self-Multipath Decoupled Antenna Pairs

To verify the effectiveness of our proposed self-multipath counteraction method, we first construct the first single-band self-multipath decoupled antenna pair with the shorted end without using any additional decoupling structures, as shown in Fig. 3(a), where the right end of Ant2 is grounded. In such a design, the length of Ant1 can be designed in different values, and $n = 1$ is chosen in (2) and (12) to make Ant2 work at half-wavelength mode. We can observe in Fig. 3(b) that the single-band1 self-multipath decoupled antenna pair would be self-decoupled at 3.5 GHz as we expected, demonstrating the effectiveness of our proposed method. However, it can be observed in Fig. 3(c) that the $\lambda/2$ mode current distribution of Ant2 would be excited and that very little energy would be coupled to the other port from the feeding port.

Fig. 4 demonstrates the tuning method of the self-decoupling frequency. We can observe that the self-decoupling frequency would not be affected by the length L_1 of Ant1 and

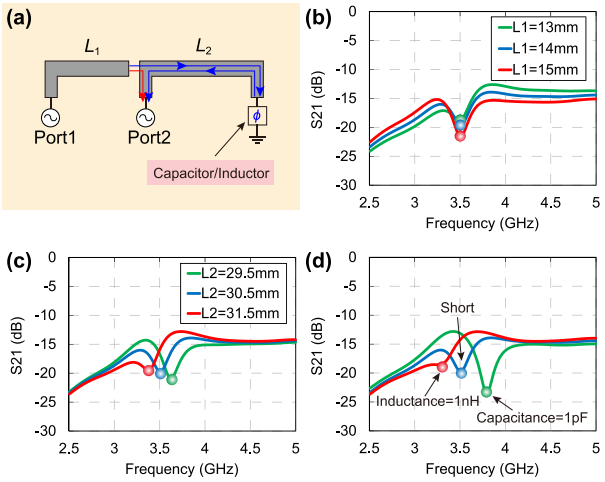

Fig. 4. Decoupling performance with different antenna parameters of the single-band1 self-multipath decoupled antenna pair. (a) Antenna parameters. (b) S_{21} with different L_1 values. (c) S_{21} with different L_2 values. (d) S_{21} with different grounded lumped elements.

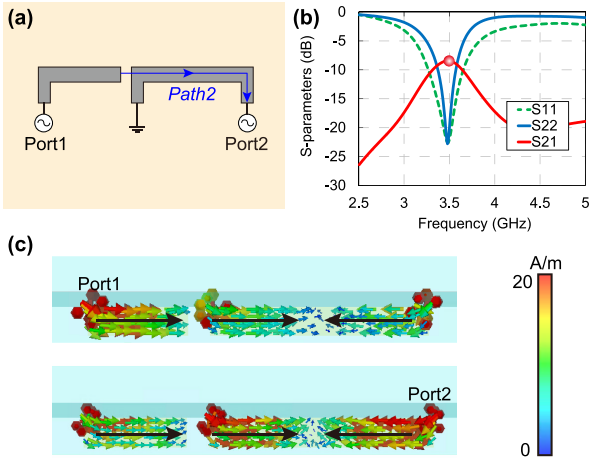

Fig. 5. Reference antenna pair without self-multipath counteraction. (a) Antenna structure. (b) S-parameters. (c) Surface current distributions at 3.5 GHz.

can be tuned by the length L_2 of Ant2. However, a lumped element of a capacitor or an inductor can be inserted at the grounding point to generate the tunable reflection phase of ϕ to replace a fixed value of π, where the self-decoupling frequency can be tuned up and down by a capacitive element and an inductive element, respectively.

It should be noticed that the feeding port and the grounding point of Ant2 cannot be interchanged even if the $\lambda/2$ mode current distribution of Ant2 is symmetrical. For example, Fig. 5(a) demonstrates the reference antenna pair when Port2 and the grounding point of Ant2 are interchanged. We can observe in Fig. 5(b) that there is no self-decoupling performance of the reference antenna pair. However, we can also observe in Fig. 5(c) that strong current would be excited on Ant1 when Port2 is fed, even though Ant2 has similar current distribution as in Fig. 3(c). And this is because path1 cannot be created when Port2 is far away from Ant1, resulting in the disappearance of the self-multipath counteraction effect.

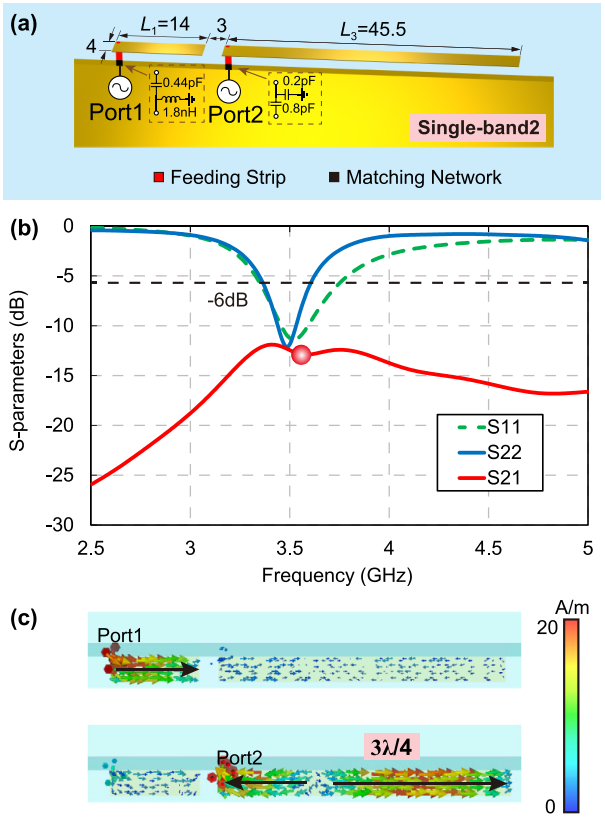

Fig. 6. Single-band2 self-multipath decoupled antenna pair. (a) Antenna structure. (b) S-parameters. (c) Surface current distributions at 3.5 GHz.

Similar to the first single-band self-multipath decoupled antenna pair in Fig. 3, we then construct the second single-band self-multipath decoupled antenna pair with the open end of Ant2, as shown in Fig. 6(a). In such a design, the length of Ant1 can also be designed in different values, and $m = 1$ is chosen in (5) and (14) to make Ant2 work at three-quarter wavelength mode. We can observe in Fig. 6(b) and (c) that the single-band2 self-multipath decoupled antenna pair would be self-decoupled at 3.5 GHz while Ant2 works at the $3\lambda/4$ mode, which further verifies the effectiveness of our proposed method.

The isolation level in Figs. 3 and 6 is different at 3.5 GHz, which is because the amplitudes of the two decoupling paths are different due to the radiation of Ant2. However, both the impedance bandwidth and the decoupling bandwidth are relatively narrow, which requires to be further widened.

IV. Dual-Band Self-Multipath Decoupled Antenna Pair

By combining the multipath of both single-band1 and single-band2 antenna pairs, we can further construct the dual-band self-multipath decoupled antenna pair through our proposed self-multipath counteraction method, as shown in Fig. 7. For the design of Ant2, both the grounding point and the open end are included in the antenna structure, and a lumped element can be inserted at the grounding point to generate the tunable reflection phase of ϕ. Through such a design, dual modes can be excited to widen the impedance bandwidth

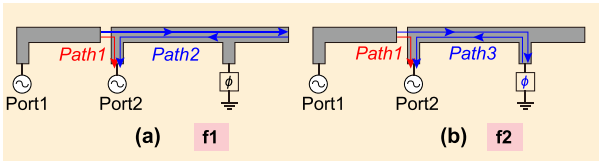

Fig. 7. Schematic of the dual-band self-decoupling paths. (a) Decoupling frequency1. (b) Decoupling frequency2.

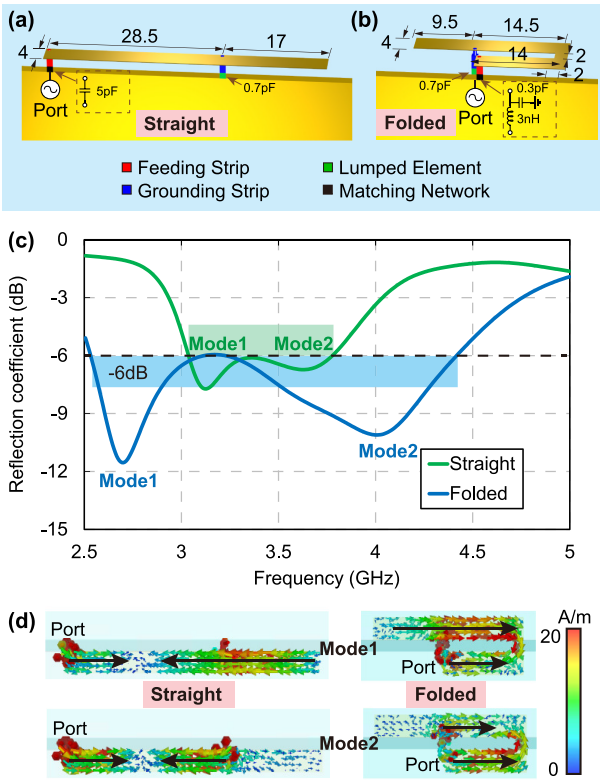

Fig. 8. Design of antenna element with wideband impedance bandwidth of only Ant2. (a) Straight antenna structure. (b) Folded antenna structure. (c) Reflection coefficients. (d) Surface current distributions.

of Ant2, and three self-decoupling paths on Ant2 are created to realize dual-band self-decoupling performance. Path1 and path2 are counteracted at the first decoupling frequency that can be tuned by the total length of Ant2, and path1 and path3 are counteracted at the second decoupling frequency that can be tuned by either the reflection phase of ϕ at the grounding point or the length of Ant2 from Port2 to the grounding point.

However, to further widen the impedance bandwidth, we shape Ant2 from a straight structure into a folded structure, as shown in Fig. 8(a) and (b). In the application of mobile terminals, $S_{11} < -6$ dB [voltage standing wave ratio (VSWR) < 3] is generally considered as a good impedance matching. On the one hand, we can observe in Fig. 8(c) that the -6 dB impedance bandwidth of the straight antenna element is improved by combining dual modes compared with Figs. 3 and 6. On the other hand, we can also observe that the -6 dB impedance bandwidth is from 3.1 to 3.8 GHz for the straight antenna structure and from 2.6 to 4.4 GHz for the folded antenna structure. Clearly, the impedance bandwidth of the antenna element is greatly improved from 700 to 1800 MHz

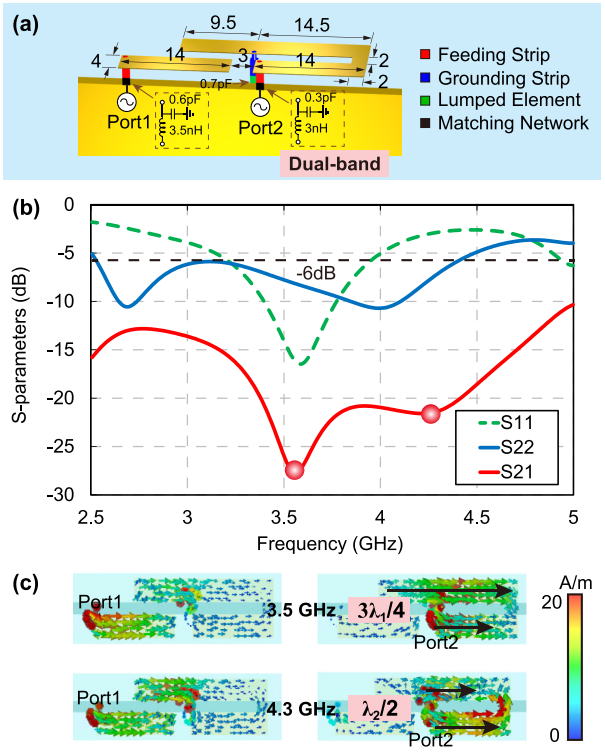

Fig. 9. Dual-band self-multipath decoupled antenna pair. (a) Antenna structure. (b) S-parameters. (c) Surface current distributions.

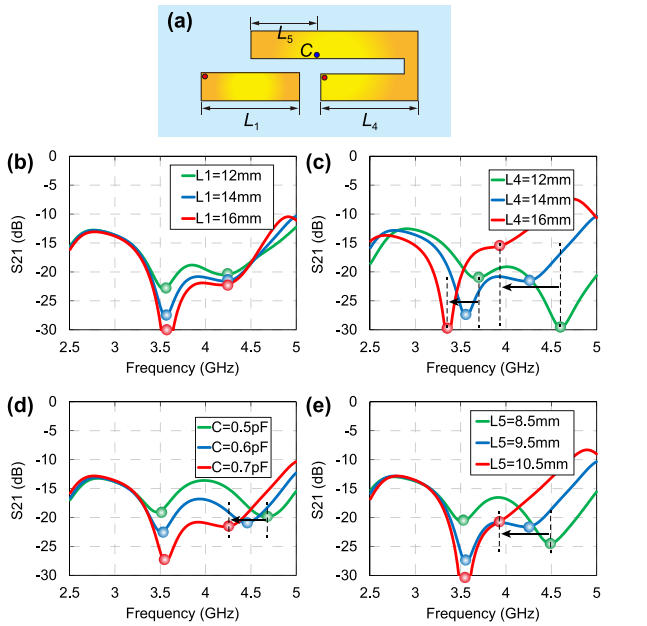

Fig. 10. Decoupling performances with different antenna parameters of the dual-band self-multipath decoupled antenna pair. (a) Antenna parameters. (b) S_{21} with different L_1 values. (c) S_{21} with different L_4 values. (d) S_{21} with different C values. (e) S_{21} with different L_5 values when the total length of Ant2 is unchanged.

when the structure is folded. As shown in Fig. 8(d), there are two resonant modes that can be excited for both the straight and the folded antenna elements. The first mode is $3\lambda/4$ mode from the feeding port to the open end, and the second mode is $\lambda/2$ mode from the feeding port to the grounding point. The change from the straight to the folded structures is that the opposite vector directions would become the same vector directions of the current distribution for both modes. Such same vector directions of the current distribution would enhance the radiation ability of the antenna element instead of canceling the radiation for the opposite vector directions, which is the reason for the bandwidth expansion of the folded antenna element. Therefore, we can obtain a wider impedance bandwidth by combining dual modes and folding the antenna structure together.

Fig. 9(a) demonstrates the dual-band self-multipath decoupled antenna pair according to the analysis of Fig. 7, where the folded structure of Ant2 in Fig. 8(b) is employed to widen the impedance bandwidth. We can observe in Fig. 9(b) that the antenna pair can be self-decoupled at both 3.5 and 4.3 GHz, demonstrating a wideband self-decoupling performance as we designed. However, we can also observe that Ant2 works at a wideband impedance bandwidth from 2.6 to 4.3 GHz, which is because the folded antenna structure of Ant2 is employed. Although an additional coupling path is generated to couple the power from Ant1 to the open end of Ant2, this coupling power is much smaller than the direct coupling power from Ant1 to Port2, which has little influence on the decoupling performance. As shown in Fig. 9(c), the current at the first decoupling frequency is distributed on path2 and exhibits the $3\lambda_1/4$ mode from the feeding port to the open end when Port2 is excited, and the current at the second decoupling frequency is distributed on path3 and exhibits the $\lambda_2/2$ mode from the feeding port to the grounding point when Port2 is excited.

Similar to the single-band1 self-multipath decoupled antenna pair in Fig. 4, we can tune the first self-decoupling frequency by the total length of Ant2 and the second self-decoupling frequency by both the reflection phase ϕ of the grounding point and the location of the grounding point of Ant2. For instance, Fig. 10 demonstrates the decoupling performance with different antenna parameters of the dual-band self-multipath decoupled antenna pair. First, both self-decoupled frequencies would not be affected by the length L_1 of Ant1 in Fig. 10(b). Second, both frequencies can be tuned by the length L_4 of Ant2 in Fig. 10(c), which is because both path2 and path3 include this branch section of Ant2. Finally, the second decoupling frequency can be tuned by either the capacitance at the grounding point in Fig. 10(d) or the location of the grounding point of Ant2 in Fig. 10(e), which is because path3 can pass through the grounding point and be reflected with the phase ϕ.

V. Four-Band Self-Multipath Decoupled Antenna Pair

Since the self-decoupled frequencies would not be affected by Ant1 in the single-band and dual-band antenna pairs mentioned earlier, we can design the type of Ant1 of the dual-band self-multipath decoupled antenna pair in Fig. 9 to be a similar type to Ant2 to further widen the decoupling bandwidth. Through such a design, as shown in Fig. 11, six self-decoupling paths are created with three on Ant1 and three on Ant2. And four-band self-decoupling performance can be realized through self-multipath counteraction happened

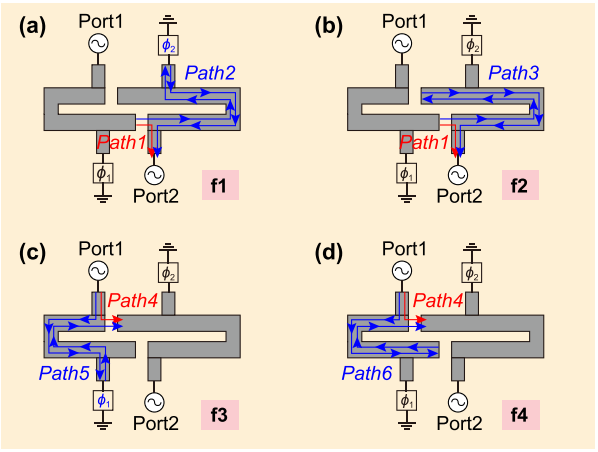

Fig. 11. Schematic of the four-band self-decoupling paths. (a) Decoupling frequency1. (b) Decoupling frequency2. (c) Decoupling frequency3. (d) Decoupling frequency4.

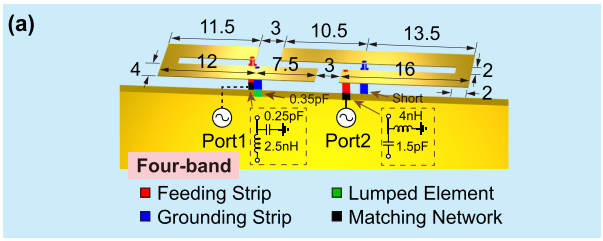

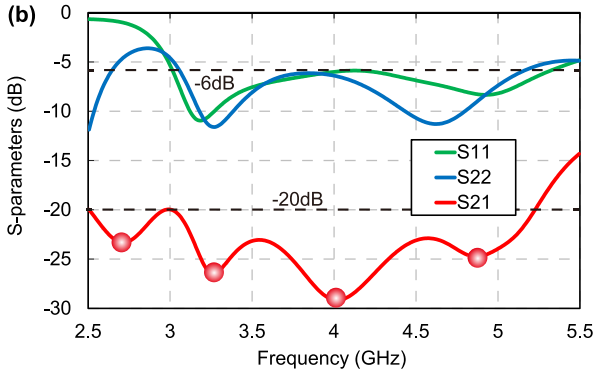

Fig. 12. Four-band self-multipath decoupled antenna pair. (a) Antenna structure. (b) S-parameters.

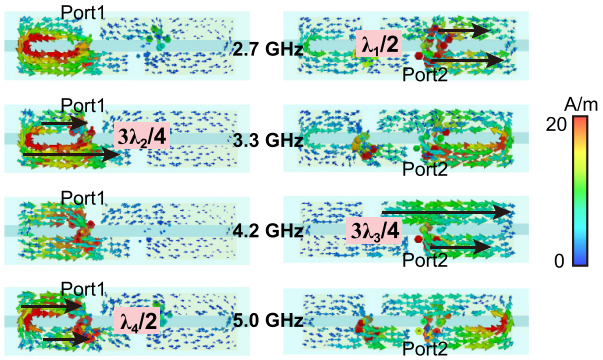

Fig. 13. Surface current distributions of the four-band self-multipath decoupled antenna pair.

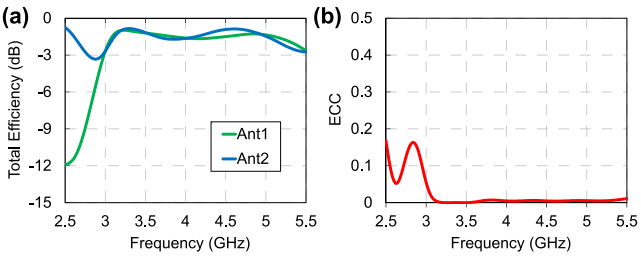

Fig. 14. (a) Antenna efficiencies. (b) ECC of the four-band self-multipath decoupled antenna pair.

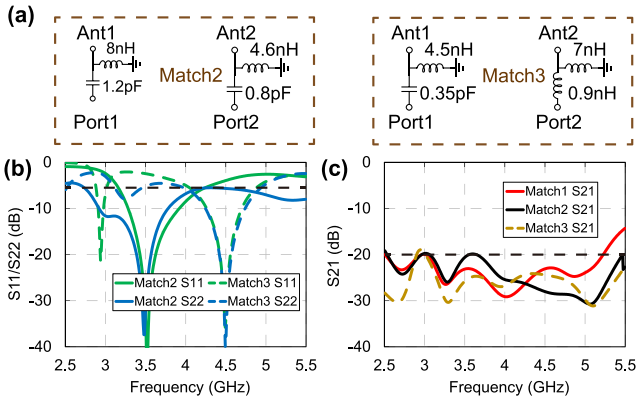

Fig. 15. Influence of the matching networks, where match1 refers to the matching networks in Fig. 12.

on both Ant1 and Ant2, where two of the self-decoupling frequencies are mainly determined by Ant2 and the other two self-decoupling frequencies are mainly determined by Ant1.

Fig. 12(a) demonstrates our proposed four-band self-multipath decoupled antenna pair according to the analysis of Fig. 11, where Ant1 is designed to be of a similar type to Ant2 but with different antenna parameters. We can observe in Fig. 12(b) that both Ant1 and Ant2 have the -6 dB impedance bandwidth from 3.1 to 5.1 GHz, which covers entire 5G N77, N78, and N79 bands. However, such antenna pair can be self-decoupled at 2.7, 3.3, 4.0, and 4.9 GHz with the isolation of more than 20 dB from 2.5 to 5.2 GHz, demonstrating excellent four-band and very wideband self-decoupling performance.

Fig. 13 demonstrates the surface current distributions of the four-band self-multipath decoupled antenna pair at the decoupling frequencies. We can observe that the first decoupling frequency is mainly determined by the $\lambda_1/2$ mode from Port2 to the grounding point of Ant2, the second decoupling frequency is mainly determined by the $3\lambda_2/4$ mode from Port1 to the open end of Ant1, the third decoupling frequency is mainly determined by the $3\lambda_3/4$ mode from Port2 to the open end of Ant2, and the fourth decoupling frequency is mainly determined by the $\lambda_4/2$ mode from Port1 to the grounding point of Ant1.

Fig. 14 continues to demonstrate the antenna efficiencies and envelope correlation coefficient (ECC) of the four-band self-multipath decoupled antenna pair. We can observe that the total efficiencies of both Ant1 and Ant2 are better than -1.6 dB and ECC is much less than 0.01 from 3.1 to 5.1 GHz, demonstrating excellent radiation and diversity performances.

TABLE I
COMPARISON BETWEEN MULTIBAND DECOUPLED ANTENNAS

Ref.	Decoupling Method	Isolation	Multi-Band	Bandwidth	Antenna Distance	Antenna Total Length	Symmetrical Requirement
[10]	Four Parasitic Scatterers	>20 dB	Four	8% (2.4-2.6 GHz)	$0.32\lambda_0$	$0.55\lambda_0$	No
[13]	Three Neutralization Lines	>15 dB	Three	52% (1.66-2.84 GHz)	$0.08\lambda_0$	$0.51\lambda_0$	Yes
[18]	Lumped Element+Connecting Line	>10 dB	Dual	41% (3.3-5.0 GHz)	$0.03\lambda_0$	$0.33\lambda_0$	Yes
[23]	Orthogonal Modes+Lumped Filters	>10 dB	Dual	5.7% (3.4-3.6 GHz) +2.1% (4.8-4.9 GHz)	$0.05\lambda_0$	$0.17\lambda_0$	Yes
[30]	Self-Decoupled	>17.5 dB	Dual	5.7% (3.4-3.6 GHz) +4.1% (4.8-5.0 GHz)	$0.014\lambda_0$	$0.25\lambda_0$	Yes
This work	Self-Multipath Decoupled	>20 dB	Four	49% (3.1-5.1 GHz)	$0.02\lambda_0$	$0.40\lambda_0$	No

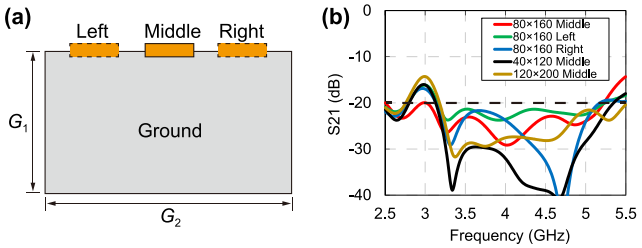

Fig. 16. Influence of the antenna location and the ground size. (a) Schematic diagram of antenna location. (b) S_{21} with different ground sizes or different positions.

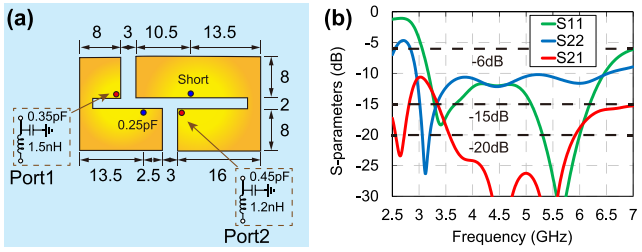

Fig. 17. Further increase in bandwidth of the four-band self-multipath decoupled antenna pair. (a) Antenna structure with the width of 8 mm. (b) S-parameters.

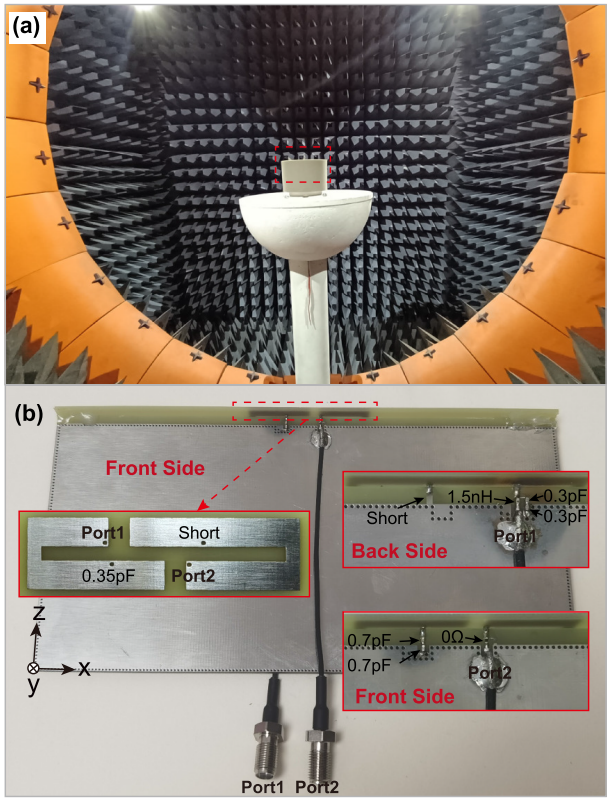

Fig. 18. Photographs of (a) measurement setup and (b) fabricated four-band self-multipath decoupled antenna pair.

The tuning method of the self-decoupling frequencies for the four-band self-multipath decoupled antenna pair is similar to the dual-band self-multipath decoupled antenna pair and can be obtained from Fig. 10. However, as shown in Fig. 15, the matching networks have very little influence on the decoupling performance when we have very small reflection coefficients at different frequencies. This is because the matching networks are in the common area of the self-decoupling paths, and the phase difference would not be changed in (3) and (6).

Fig. 16 demonstrates the influence of the antenna location and the ground size, where the antenna pair is placed at different locations on the ground or the ground is adjusted with the size of $G_1 \times G_2$. Although the isolation level is changed a little due to the radiation of the ground, excellent decoupling performance can always be obtained when the antenna pair moves and the ground size changes.

Clearly, the working bandwidth of the four-band self-multipath decoupled antenna is no longer dependent on the decoupling bandwidth but only limited by the impedance bandwidth under such a wide self-decoupling bandwidth. There are many methods to further obtain a better impedance matching and improve the impedance bandwidth. For example, Fig. 17 shows the antenna performance when the width of the antenna is increased from 4 to 8 mm. We can observe that Ant1 and Ant2 have the −6 dB impedance bandwidth from 3.3 to 7.0 GHz with the isolation more than 15 dB and from 3.6 to 5.9 GHz with the isolation more than 20 dB, demonstrating both very wide impedance bandwidth and decoupling bandwidth performances.

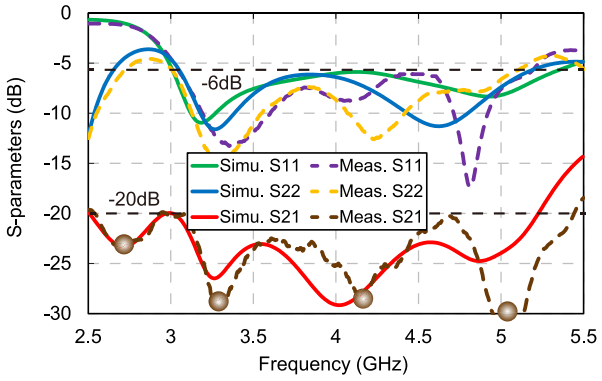

Fig. 19. Simulated and measured S-parameters of the four-band self-multipath decoupled antenna pair.

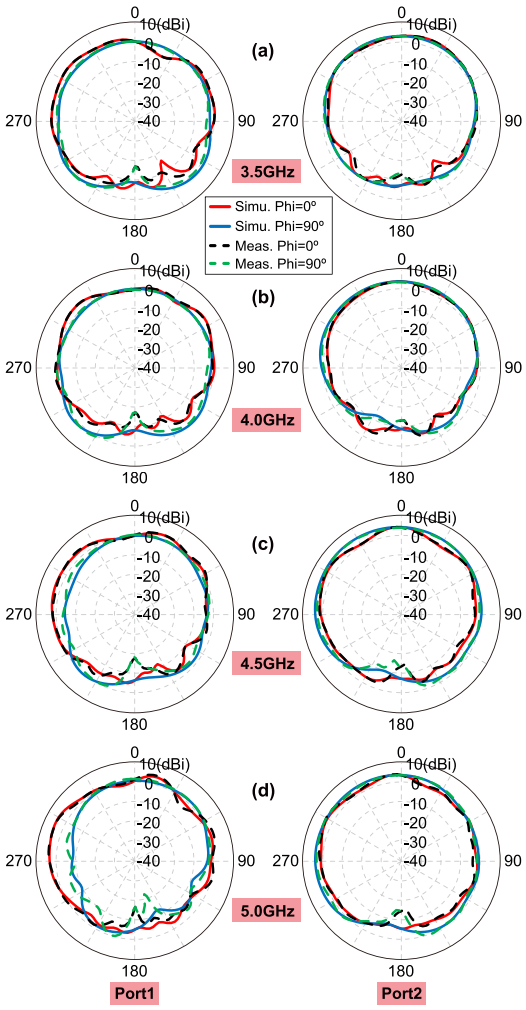

Fig. 20. Simulated and measured radiation patterns of the four-band self-multipath decoupled antenna pair. (a) 3.5 GHz. (b) 4.0 GHz. (c) 4.5 GHz. (d) 5.0 GHz.

Table I demonstrates the detailed comparison in antenna decoupling performance between multiband decoupled antennas that have been proposed. We can observe that our proposed method has many advantages than the previous studies. First, our proposed antenna pair can be self-decoupled without using any additional decoupling structures. Second, there is no antenna symmetrical requirement of our proposed method. Then, a much wider decoupling bandwidth than most of the existing studies can be achieved. Finally, excellent decoupling performance more than 20 dB of the isolation can be easily obtained over a wideband range for closely spaced antennas.

VI. Experimental Results

Finally, we fabricate a prototype of the proposed four-band self-multipath decoupled antenna pair which is formed by combining two FR4 circuit boards ($\varepsilon_r = 4.4$ and loss tangent $= 0.02$), and the radiation performance is measured in a multiprobe anechoic chamber, as shown in Fig. 18. In the prototype, two 0.7 pF capacitors are in series to be equivalent to a 0.35 pF capacitor at the grounding point. However, due to the influence of the increased footprint of the matching network, the element value of the matching network has a little adjustment to have a better impedance matching compared with the simulated model in Fig. 12.

Fig. 19 shows the simulated and measured S-parameters of the four-band self-multipath decoupled antenna pair. We can observe that the fabricated antenna pair can work from 3.1 to 5.2 GHz with the -6 dB impedance bandwidth and can be self-decoupled at 2.7, 3.3, 4.2, and 5.0 GHz with the isolation more than 20 dB from 2.6 to 5.4 GHz, which is in good agreement with the simulated results and also demonstrates excellent four-band and very wideband self-decoupling performance. However, the far-field radiation patterns in Fig. 20 show that both Ant1 and Ant2 possess the omnidirectional radiation characteristics in a wideband range, which provides excellent radiation performance for mobile terminals.

VII. Conclusion

In conclusion, we have proposed several self-multipath decoupled antenna pairs from a single decoupling band to four decoupling bands based on self-multipath counteraction method. First, we demonstrated the decoupling principle of the self-multipath counteraction method by building multiple paths on the radiating branch of one of the antennas, which was also verified by the equivalent circuit results. Then, we constructed a series of self-multipath decoupled antennas pairs that is capable of realizing self-decoupling performance from a single band to four bands. Especially, the four-band self-multipath decoupled antenna pair can be self-decoupled at a very wideband range with the isolation more than 20 dB in the -6 dB impedance bandwidth from 3.1 to 5.1 GHz, covering entire N77, N78, and N79 bands. Finally, the experiment of the four-band self-multipath decoupled antenna pair was carried out, and the measured results agreed very well with the simulated results. Our proposed decoupling method, with the merits of simple antenna structure and wideband self-decoupling performance, should provide significant application values for the very compact and wideband 5G and future 6G mobile terminals.

REFERENCES

[1] M. A. Jensen and J. W. Wallace, "A review of antennas and propagation for MIMO wireless communications," *IEEE Trans. Antennas Propag.*, vol. 52, no. 11, pp. 2810–2824, Nov. 2004.

[2] B. Qian, X. Huang, X. Chen, M. Abdullah, L. Zhao, and A. Kishk, "Surrogate-assisted defected ground structure design for reducing mutual coupling in 2×2 microstrip antenna array," *IEEE Antennas Wireless Propag. Lett.*, vol. 21, no. 2, pp. 351–355, Feb. 2022.

[3] B. Qian, X. Chen, and A. A. Kishk, "Decoupling of microstrip antennas with defected ground structure using the common/differential mode theory," *IEEE Antennas Wireless Propag. Lett.*, vol. 20, no. 5, pp. 828–832, May 2021.

[4] J. Ouyang, F. Yang, and Z. M. Wang, "Reducing mutual coupling of closely spaced microstrip MIMO antennas for WLAN application," *IEEE Antennas Wireless Propag. Lett.*, vol. 10, pp. 310–313, 2011.

[5] X.-J. Zou, G.-M. Wang, Y.-W. Wang, and H.-P. Li, "An efficient decoupling network between feeding points for multielement linear arrays," *IEEE Trans. Antennas Propag.*, vol. 67, no. 5, pp. 3101–3108, May 2019.

[6] L. Zhao, L. K. Yeung, and K.-L. Wu, "A coupled resonator decoupling network for two-element compact antenna arrays in mobile terminals," *IEEE Trans. Antennas Propag.*, vol. 62, no. 5, pp. 2767–2776, May 2014.

[7] Y.-M. Zhang, S. Zhang, J.-L. Li, and G. F. Pedersen, "A transmission-line-based decoupling method for MIMO antenna arrays," *IEEE Trans. Antennas Propag.*, vol. 67, no. 5, pp. 3117–3131, May 2019.

[8] S. C. Chen, Y. S. Wang, and S. J. Chung, "A decoupling technique for increasing the port isolation between two strongly coupled antennas," *IEEE Trans. Antennas Propag.*, vol. 56, no. 12, pp. 3650–3658, Dec. 2008.

[9] B. K. Lau and J. B. Andersen, "Simple and efficient decoupling of compact arrays with parasitic scatterers," *IEEE Trans. Antennas Propag.*, vol. 60, no. 2, pp. 464–472, Feb. 2012.

[10] H. Xu, H. Zhou, S. Gao, H. Wang, and Y. Cheng, "Multimode decoupling technique with independent tuning characteristic for mobile terminals," *IEEE Trans. Antennas Propag.*, vol. 65, no. 12, pp. 6739–6751, Dec. 2017.

[11] A. Diallo, C. Luxey, P. L. Thuc, R. Staraj, and G. Kossiavas, "Study and reduction of the mutual coupling between two mobile phone PIFAs operating in the DCS1800 and UMTS bands," *IEEE Trans. Antennas Propag.*, vol. 54, no. 11, pp. 3063–3074, Nov. 2006.

[12] S.-W. Su, C.-T. Lee, and F.-S. Chang, "Printed MIMO-antenna system using neutralization-line technique for wireless USB-dongle applications," *IEEE Trans. Antennas Propag.*, vol. 60, no. 2, pp. 456–463, Feb. 2012.

[13] Y. Wang and Z. Du, "A wideband printed dual-antenna with three neutralization lines for mobile terminals," *IEEE Trans. Antennas Propag.*, vol. 62, no. 3, pp. 1495–1500, Mar. 2014.

[14] C. Deng, D. Liu, and X. Lv, "Tightly arranged four-element MIMO antennas for 5G mobile terminals," *IEEE Trans. Antennas Propag.*, vol. 67, no. 10, pp. 6353–6361, Oct. 2019.

[15] L. Sun, Y. Li, and Z. Zhang, "Decoupling between extremely closely spaced patch antennas by mode cancellation method," *IEEE Trans. Antennas Propag.*, vol. 69, no. 6, pp. 3074–3083, Jun. 2021.

[16] J. Sui, Y. Dou, X. Mei, and K.-L. Wu, "Self-curing decoupling technique for MIMO antenna arrays in mobile terminals," *IEEE Trans. Antennas Propag.*, vol. 68, no. 2, pp. 838–849, Feb. 2020.

[17] A. Zhang, K. Wei, S. Chu, and Y. Wang, "Extremely compact interconnected half-mode cavity antennas with enhanced isolation for MIMO system," *IEEE Trans. Antennas Propag.*, vol. 70, no. 12, pp. 12264–12269, Dec. 2022.

[18] L. Sun, Y. Li, and Z. Zhang, "Wideband integrated quad-element MIMO antennas based on complementary antenna pairs for 5G smartphones," *IEEE Trans. Antennas Propag.*, vol. 69, no. 8, pp. 4466–4474, Aug. 2021.

[19] L. Sun, Y. Li, and Z. Zhang, "Wideband decoupling of integrated slot antenna pairs for 5G smartphones," *IEEE Trans. Antennas Propag.*, vol. 69, no. 4, pp. 2386–2391, Apr. 2021.

[20] L. Chang, Y. Yu, K. Wei, and H. Wang, "Orthogonally polarized dual antenna pair with high isolation and balanced high performance for 5G MIMO smartphone," *IEEE Trans. Antennas Propag.*, vol. 68, no. 5, pp. 3487–3495, May 2020.

[21] L. Chang, Y. Yu, K. Wei, and H. Wang, "Polarization-orthogonal co-frequency dual antenna pair suitable for 5G MIMO smartphone with metallic bezels," *IEEE Trans. Antennas Propag.*, vol. 67, no. 8, pp. 5212–5220, Aug. 2019.

[22] Z. Xu and C. Deng, "High-isolated MIMO antenna design based on pattern diversity for 5G mobile terminals," *IEEE Antennas Wireless Propag. Lett.*, vol. 19, no. 3, pp. 467–471, Mar. 2020.

[23] L. Chang, G. Zhang, and H. Wang, "Dual-band antenna pair with lumped filters for 5G MIMO terminals," *IEEE Trans. Antennas Propag.*, vol. 69, no. 9, pp. 5413–5423, Sep. 2021.

[24] L. Sun, Y. Li, Z. Zhang, and Z. Feng, "Wideband 5G MIMO antenna with integrated orthogonal-mode dual-antenna pairs for metal-rimmed smartphones," *IEEE Trans. Antennas Propag.*, vol. 68, no. 4, pp. 2494–2503, Apr. 2020.

[25] A. Zhang, K. Wei, S. Chu, Q. Guan, and Y. Hu, "Low-profile patch antenna pair with pattern diversity using common and differential modes for MIMO systems," *IEEE Antennas Wireless Propag. Lett.*, vol. 21, no. 10, pp. 1935–1939, Oct. 2022.

[26] L. Sun, Y. Li, Z. Zhang, and H. Wang, "Antenna decoupling by common and differential modes cancellation," *IEEE Trans. Antennas Propag.*, vol. 69, no. 2, pp. 672–682, Feb. 2021.

[27] L. Sun, Y. Li, Z. Zhang, and H. Wang, "Self-decoupled MIMO antenna pair with shared radiator for 5G smartphones," *IEEE Trans. Antennas Propag.*, vol. 68, no. 5, pp. 3423–3432, May 2020.

[28] A. Zhang, K. Wei, Y. Hu, and Q. Guan, "High-isolated coupling-grounded patch antenna pair with shared radiator for the application of 5G mobile terminals," *IEEE Trans. Antennas Propag.*, vol. 70, no. 9, pp. 7896–7904, Apr. 2022.

[29] K.-L. Wong, C.-Y. Tsai, and J.-Y. Lu, "Two asymmetrically mirrored gap-coupled loop antennas as a compact building block for eight-antenna MIMO array in the future smartphone," *IEEE Trans. Antennas Propag.*, vol. 65, no. 4, pp. 1765–1778, Apr. 2017.

[30] Z. Ren and A. Zhao, "Dual-band MIMO antenna with compact self-decoupled antenna pairs for 5G mobile applications," *IEEE Access*, vol. 7, pp. 82288–82296, 2019.

[31] J. Sui and K.-L. Wu, "A self-decoupled antenna array using inductive and capacitive couplings cancellation," *IEEE Trans. Antennas Propag.*, vol. 68, no. 7, pp. 5289–5296, Jul. 2020.

[32] H. Lin, Q. Chen, Y. Ji, X. Yang, J. Wang, and L. Ge, "Weak-field-based self-decoupling patch antennas," *IEEE Trans. Antennas Propag.*, vol. 68, no. 6, pp. 4208–4217, Jun. 2020.

[33] D. M. Pozar, *Microwave Engineering*. Hoboken, NJ, USA: Wiley, 2011.

Aofang Zhang (Member, IEEE) received the B.S. degree in electromagnetic wave propagation and antenna and the Ph.D. degree in electromagnetic field and microwave technology from Xidian University, Xi'an, China, in 2014 and 2019, respectively.

From 2019 to 2020, he was with the Consume Business Group, Huawei Technologies Company Ltd., Xi'an. In 2021, he joined Honor Device Company Ltd., Xi'an, where he is currently a Senior Expert for the antenna design of smartphones, tablets, laptops, and routers. His current interests include antenna decoupling, multiband antennas, small size antennas, and MIMO antennas.

Kunpeng Wei (Senior Member, IEEE) received the B.S. degree in electronic and information engineering from the Huazhong University of Science and Technology, Wuhan, China, in 2008, and the Ph.D. degree in electrical engineering from Tsinghua University, Beijing, China, in 2013.

From July 2013 to December 2015, he was with the Radar Research Institute of Chinese Air Force Research Laboratory, conducting research in the areas of phased-array antenna design and radar system design. He joined the Consume Business Group, Huawei Inc., in 2016, where he had been an Antenna Specialist and the Director of Xi'an Antenna Team for 5 years. Since 2021, he has been with Honor Device Company Ltd., when this company split from Huawei and he was the Director of Honor Antenna Team. After leaving Honor, he joined Xiaomi Corporation, Beijing, in 2023. He is currently the Chief Antenna Expert and the Head of the Antenna Technology Team. He is a special level external expert of the China Academy of Information and Communications Technology. He is also an Adjunct Professor with School of Electronics and information engineering, Shenzhen University, Shenzhen, China. He leads a large group of antenna experts and engineers and takes the full responsibility in the research of antenna technologies to guarantee the market success of all Xiaomi's products ranging from smartphones, electric cars, tablets, laptops, and other IOT devices. He has authored over 50 refereed papers on consumer electronics antenna design. He holds over 50 granted U.S./EU/JP/CN patents and has more than 20 other patent applications in pending. His current research interests include meta-antennas, smart-phone antenna design, small-size 5G antenna systems in terminal device, and millimeter-wave antenna array.

Dr. Wei is an IET Fellow. He was a recipient of the Principal Scholarship of Tsinghua University in 2012, the Huawei Individual Gold Medal Award in 2018, the Huawei Team Gold Medal Award in 2017, and the Honor Team Gold Medal Award in 2021. He has been serving as an Associate Editor for *IET ELECTRONICS LETTERS* since October 2021.

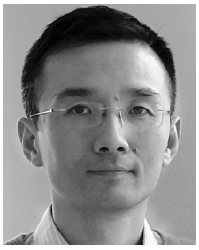

Zhijun Zhang (Fellow, IEEE) received the B.S. and M.S. degrees from the University of Electronic Science and Technology of China, Chengdu, China, in 1992 and 1995, respectively, and the Ph.D. degree from Tsinghua University, Beijing, China, in 1999.

In 1999, he was a Post-Doctoral Fellow with the Department of Electrical Engineering, University of Utah, Salt Lake City, UT, USA, where he was appointed as a Research Assistant Professor in 2001. In May 2002, he was an Assistant Researcher with the University of Hawaii at Manoa, Honolulu, HI, USA. In November 2002, he joined Amphenol T&M Antennas, Vernon Hills, IL, USA, as a Senior Staff Antenna Development Engineer and was then promoted to the position of Antenna Engineer Manager. In 2004, he joined Nokia Inc., San Diego, CA, USA, as a Senior Antenna Design Engineer. In 2006, he joined Apple Inc., Cupertino, CA, USA, as a Senior Antenna Design Engineer and was then promoted to the position of Principal Antenna Engineer. Since August 2007, he has been with Tsinghua University, where he is currently a Professor with the Department of Electronic Engineering. He is the author of *Antenna Design for Mobile Devices* (Wiley, First Edition 2011 and Second Edition 2017).

Dr. Zhang served as an Associate Editor for the IEEE TRANSACTIONS ON ANTENNAS AND PROPAGATION from 2010 to 2014 and the IEEE ANTENNAS AND WIRELESS PROPAGATION LETTERS from 2009 to 2015.